AN X-RAY STUDY OF LATTICE STRAIN VARIATION IN LOW CARBON STEEL

by

Comondore Ravindran

A Thesis Submitted in Partial Fulfillment of
The Requirements for the Degree of
Master of Science

The Faculty of Graduate Studies and Research
Department of Mechanical Engineering
University of Manitoba

July, 1970

ABSTRACT

Simultaneous measurements of lattice [elastic] strain by the x-ray line shift method and total strain with an electrical strain gauge have been carried out on SAE 1010 steel with the help of a special tensometer-attachment to the X-ray diffractometer.

The particular features investigated are: The variation of the lattice strain and the total strain with applied stress above the limit of proportionality, the effect [in detail] of the mode of unloading on the lattice strain and the total strain and the contribution of the intergranular stresses and the stacking faults to X-ray line shifts.

ACKNOWLEDGEMENTS

The author is grateful to his Research Supervisor, Professor K. Tangri, for his advice and encouragement at all stages of this work. Helpful discussions with Dr. R. T. Holt are also sincerely acknowledged.

Thanks are extended to Mr. D. Mardis for technical assistance.

TABLE OF CONTENTS

LIST OF FIGURES

LIST OF TABLES

1. INTRODUCTION AND OBJECTIVE

Careful experiments have led to the recognition of residual lattice strains [RLS] in deformed polycrystalline aggregates. The early observations of this effect have been reported by Wever and Pfarr[1] in 1933, Bollenrath et al[2] in 1939, and Smith and Wood[3,4] in 1941-42.

Various explanations[5] have been advanced to explain the lattice strain effects accompanying the plastic deformation of polycrystals. The basic principle common to all these is as follows. It is assumed that different parts of the aggregate have different yield stresses. Assuming that part A yields at much lower applied stress than part B, subsequent to the process of deformation, the elastic strain in A will be less than that in B. On removal of the applied stress, B will tend to contract further than A but will be prevented from doing so by the restraining influence of A. The state of final equilibrium is such that A is in compression and B in tension. The argument can be extended to a large number of different parts. While this reasoning is tacitly accepted in principle, there appears to be a controversy as to the exact nature of parts A and B.

Bollenrath and his co-workers[2] have plastically extended a mild steel specimen and have observed the residual lattice strain at surfaces successively exposed by etching away layers of the metal. They point out that grains in the free surface of a polycrystalline metal are less restrained than those in the interior and that the former on the average should have a lower yield stress than the latter.

This view is supported to some extent by Glocker and Hasenmaier[6], and contradicted by Smith and Wood[7].

Greenough[5][based on an earlier interpretation by Heyn and Masing] has proposed that different grains would have different yield stresses depending on their orientations. They have found that the intergranular stresses [Heyn intergranular stresses] do make a large contribution to the observed residual lattice strains. However, it is presumed that there must be, in addition, some other effect such as a surface macroscopic stress since all the observed strains are more positive than anticipated. Further, while it is agreed that the residual lattice strain in crystals of one orientation would vary as the orientations of the neighbouring crystals varied, it is pointed out that the average strain taken over many grains of the particular orientation would not be zero, but would depend on the difference of the yield stress of the grain with the given orientation and the average yield stress of the aggregate. Experimental evidences in favour of this argument have been given for iron and steel by Garrod[8] and by Finch[9].

Newton and Vacher[10] have studied residual lattice strains in sectioned bars of plastically deformed iron, and their observations seem to be more in line with the suggestions that the highly distorted material at or near crystal boundaries is the harder part rather than the suggestion that the harder part is an adjacent crystal of different orientation. However, it is pointed by Donachie and Norton[11] that residual lattice strains do not arise in any detectable manner from a macroscopic stess system, and they are not solely,

or in major part, the result of an intergranular stress system.

Garrod and Hawkes[12] have investigated the possible contributory processes to the residual lattice strains in iron and mild steel. They do not find any evidence for significant intergranular system of Heyn stresses. In addition, they believe that no single mechanism could be invoked to explain the results. According to them at least three and possibly four processes are significant in the case of mild steel.

A macroscopic surface effect[2] is expected to result from the different yield stresses of the surface and the interior of a polycrystalline metal. A modification of the above concept suggests that in the plastic range, the surface layer will on the average harden less rapidly than the core[13,14]. Whereas, however, the surface effect should produce a surface stress which is independent of the amount of plastic deformation, the stress due to the hardening effect should increase with increasing deformation. If the material contains more than one phase with different yield strengths, a pseudo-macroscopic effect[15] results. For the X-ray measurements on a given reflection from one phase would indicate a macroscopic stress in that phase due to this cause.

Garrod and Hawkes[11] suggested a model based on the hypothesis originally advanced by Smith and Wood[7] in which the residual lattice strains were attributed to the high-strength grain boundaries. After heavy deformation, each grain in the polycrystalline aggregate is composed of a number of polycrystals with mis-orientations of a few degrees between neighbours and with a non-uniform distribution of dislocations. On this model, the boundaries between particles

are not narrow discontinuities in the lattice but wider volumes in which concentrated dislocation pile-ups, associated with intersecting slip bands or walls of screw dislocations, form highly distorted regions which are presumably principal sites of the strain-hardening observed in cold-worked material. It is suggested by Garrod and Hawkes[12] that these regions act as a harder phase than the interior of the particles and produce a pseudo-macroscopic stress system analogous to the inter-phase effect suggested by Hauk[15].

Bragg, Orowan, Smith and Wood[16] have suggested a model based on the possibility that during the process of plastic deformation, the accumulation of dislocations around obstacles to their propagation through the crystal would cause higher stresses in the region of accumulation of dislocations than in the remaining bulk of the crystal. After removal of the applied stress, these regions of accumulated dislocations are left in a state of tensile stress, these stresses being balanced by those in the bulk of the crystal remote from the dislocations.

Auld and Greenough[17] have found that single crystals of iron do not show residual lattice strains after plastic extension. This is interpreted as showing that the residual lattice strains observed in polycrystalline iron are due to an intergranular stress system rather than due to stresses associated with trapped dislocations.

It should be observed that several workers[5] have assumed that the residual lattice strain observed in unloaded specimens is related to the lack of proportionality between lattice strain and applied stress in the region above the yield stress.

While attempting to draw a distinction between the regions of opposing stresses, it has been observed by C. J. Newton[18], and more recently by Cullity[19], that the regions of high density of dislocations could constitute the harder regions as opposed to the softer regions which could as well be the interior of grains. Keh and Weissmann[20] have produced a series of micrographs showing the progressive changes which occur during the plastic deformation of iron. As plastic deformation proceeds, more and more dislocations appear ultimately culminating in a tagled web of dislocations that delineate a cell structure. Cullity identifies the walls of these cells with regions subjected to a large tensile stress and the subgrains having a nearly constant and a very low dislocation density with regions stressed more or less uniformly in compression. A similar proposal has also been made by Garrod and Coyle[21].

Recently, Swaroop and Tangri[22] have performed simultaneous measurements of total strain in the direction of pulling and lattice strain normal to the direction of pulling on polycrystalline nickel with the help of a special tensometer attachment for the X-ray diffractometer. They have found that, during the initial stages of deformation, the rate of increase in lattice strain closely follows the total strain until the plastic strain sets in. From then onwards, the two strains have been found to deviate from each other, the rate of increase in lattice strain eventually decreasing with increase in applied stress. The specimens pulled to a total strain within the proportionality limit have been found to show no residual lattice or total strains. Furthermore, depending on the mode of unloading, both

compressive and tensile strains have been observed up to a deformation of 0.29% strain. Specimens gradually unloaded over a period of time have been found to show residual lattice strains of a compressive nature, while those instantaneously unloaded showed residual lattice strains of a tensile nature which reverted to a compressive nature on aging at room temperature. These results have been explained on the basis of effects of clustering of dislocations and also the production and behavior of point defects during loading and unloading respectively.

While the above review depicts the various attempts that have been made with a view to elucidate the nature and the origin of the residual lattice strain, no clear understanding has developed yet as to the behavior of lattice strain effects above the limit of proportionality. Furthermore, Swaroop and Tangri[22] have drawn attention to the nature of the lattice strain during and after gradual unloading, and also to the variation in the residual lattice strain with time in the specimens that have been instantaneously unloaded subsequent to deformation to various extents of total strain.

It was pointed out that several authors[18,19,21,22] have tried to relate the origin of the residual lattice strain to the dislocation substructures produced during deformation, and these are supposed to constitute regions of stress opposite in sign to the coherently diffracting domains which essentially form the bulk of the material. An investigation of such a mechanism calls for a study of X-ray background intensity with deformation which is due to the incoherently scattering domains such as the grain boundaries or tangles of dislocations.

Under these circumstances, the objectives of the present investigation are:

(a) To ascertain the behavior of the lattice strain up to about 1.35% strain, with particular interest in the behavior above the limit of proportionality, and explain the phenomenon by an appropriate hypothesis.

(b) To know the nature of the lattice strain during the process of gradual unloading.

(c) To know the stress at which the residual lattice strain originates and to study the variation in the residual lattice strain with time subsequent to instantaneous unloading.

(d) To study the variation in the X-ray background intensity, if any, and relate them to (a).

(e) To investigate into the role of stacking faults or the stem system associated with the origin of the residual lattice strain.

2. EXPERIMENTAL PROCEDURES

2.1 Properties of the Material in the As-supplied Condition.

The material for investigation was SAE 1010 steel received in the form of sheets which were aluminium killed, cold rolled and annealed with the following chemical analysis.

TABLE 1.

Chemical Analysis of the Specimen.

Element	Contents %
Carbon	0.09
Manganese	0.37
Phosphorus	0.004
Sulphur	0.043
Silicon	0.14
Copper	traces

Calculations were made to determine the relative amounts of the various phases present in the material and it was found that 90.02% of ferrite and 9.98% of pearlite were present. Of this amount of pearlite, 1.23% constituted cementite. Quantitative metallographic techniques using the method of point counting and the method of lineal analysis were found to yield almost similar values for the various phases present.

2.2 Specimen Preparation

2.2.1. Thermo-mechanical Treatments

The sheet in the as-supplied condition was cut into strips 2 inches long and 0.625 inches wide. These strips were cold-rolled down to 0.017 inch thickness and annealed at 850°C for two hours. Subsequently, an additional cold-rolling was performed, the resulting thickness of the strips being 0.014 inch. The strips were machined to give specimens [fig. 1] of required dimensions, subsequently annealed at 850°C for one hour. All the annealing operations were preceded by encapsulation of the specimens in silica tube evacuated and sealed in argon at a pressure of 1×10^{-5} Torr.

2.2.2. Electropolishing for X-ray Diffraction

Both the surfaces of the specimens were lightly polished by hand to four zeros emery papers to remove any surface blemishes and then cleaned in acetone. The specimens were then electropolished in the following solution at 15°C [to about 0.010" thickness]:

10% Orthophosphoric acid [70% concentration]

90% Glacial acetic acid

The best polishing conditions were obtained at a potential of 10-12 volts D.C. and a current of 0.6 ampere with constant stirring. The final rinsing was very critical, staining was avoided by quickly rinsing in two separate ethyl alcohol baths and preserving in acetone until use.

Five of the annealed specimens taken at random were electropolished and etched in 2% nital. The specimens were found to be fully recrystallized with an average ferritic grain size of 10.45×10^{-4} cm.

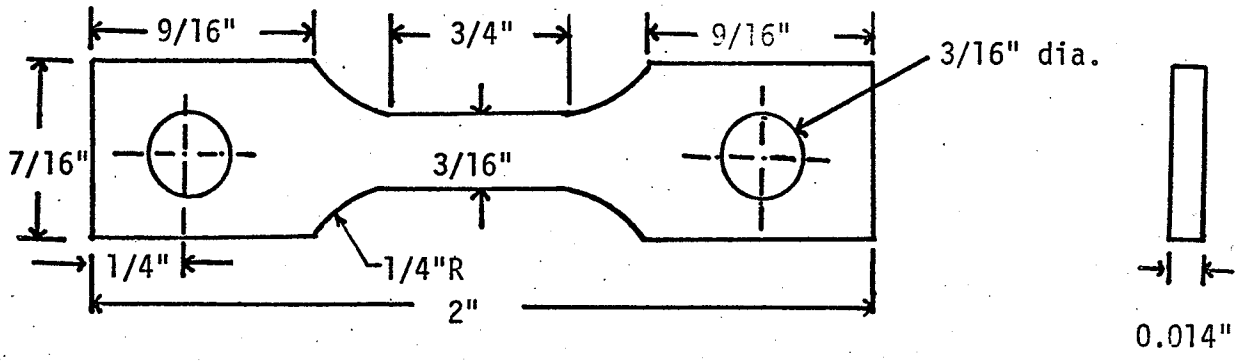

Fig. 1. Tensile Test Specimen.

as determined by planimetric method.

2.3 Tensometer-attachment for the X-ray Diffractometer.

A tensometer-attachment [figs. 2 and 3] was specially designed for the X-ray diffractometer. One of the ends of the specimen is fastened to a fixed grip, while the other is fastened to a movable grip which moves under the influence of a direct load. Thus, the essential advantage of the device is that it facilitates direct uni-axial loading and unloading of the specimen, thereby obviating the requirement of a calibrating device.

The following measurements could be made with this arrangement:

(a) The applied stress by the weights directly added on a pan connected to the movable grip through a cord.

(b) The lattice strain, e_z in a direction perpendicular to the direction of pulling [x-direction] from shifts in the X-ray peak positions [fig. 4].

(c) The total strain, ε_x in the direction of pulling, with the help of an electrical strain gauge [Budd C6-121A] affixed to the back of the specimen directly below the area irradiated by the X-rays. [The electrical strain gauge used was temperature compensated and extreme caution was exercised in the measurement of the total strain as suggested by Carnahan and White[23].]

2.4 X-ray Diffraction Procedures.

2.4.1. Measurement of Lattice Strain.

The calculated values for reflection angles for α-iron

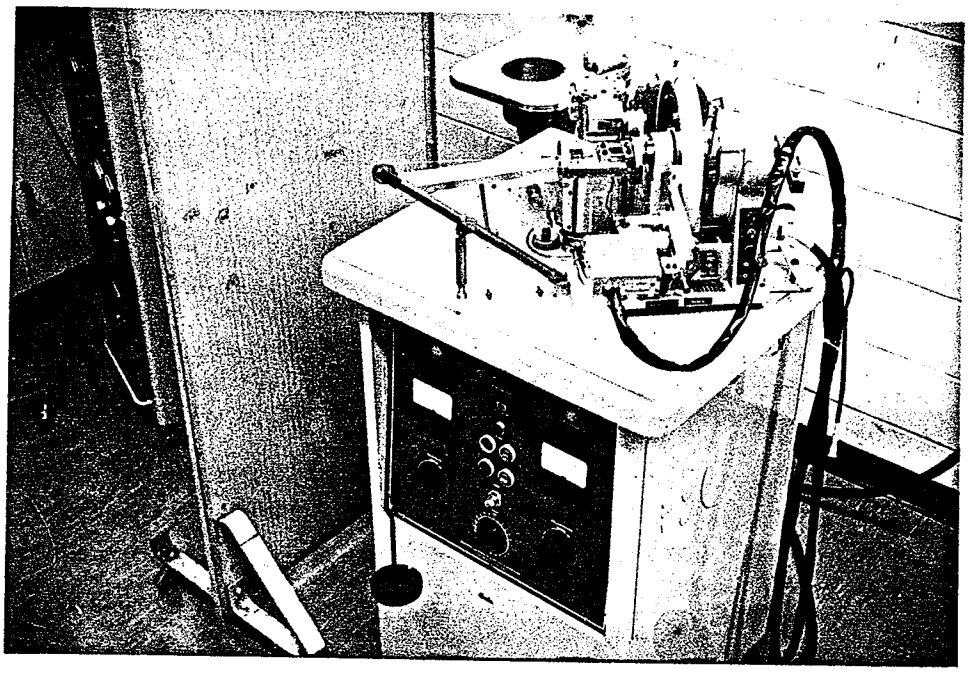

Fig. 2. X-ray Diffractometer with the tensometer-attachment including the loading device.

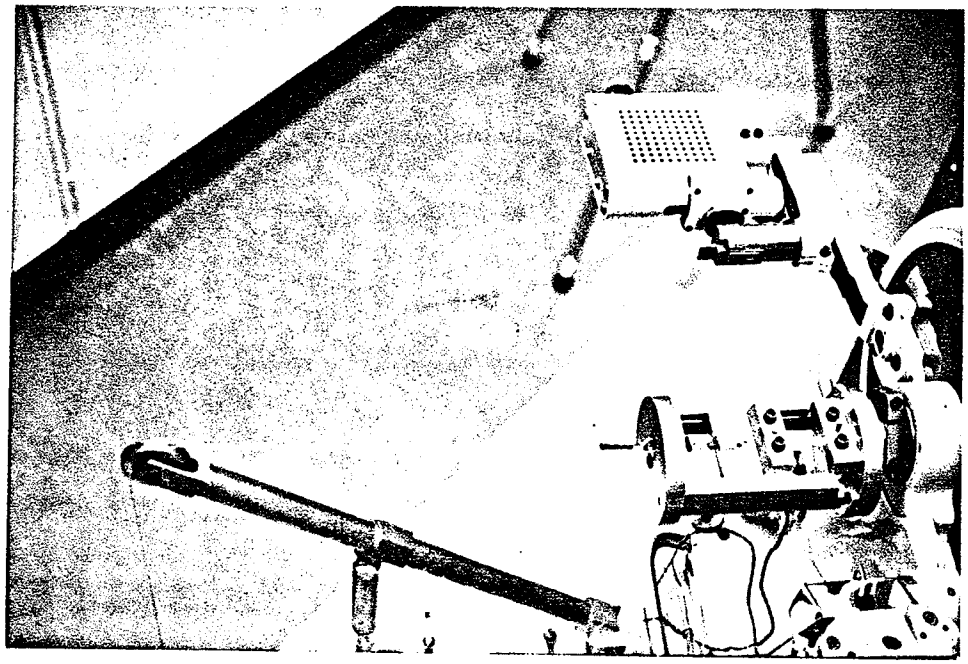

Fig. 3. Tensometer-attachment to the X-ray Diffractometer.

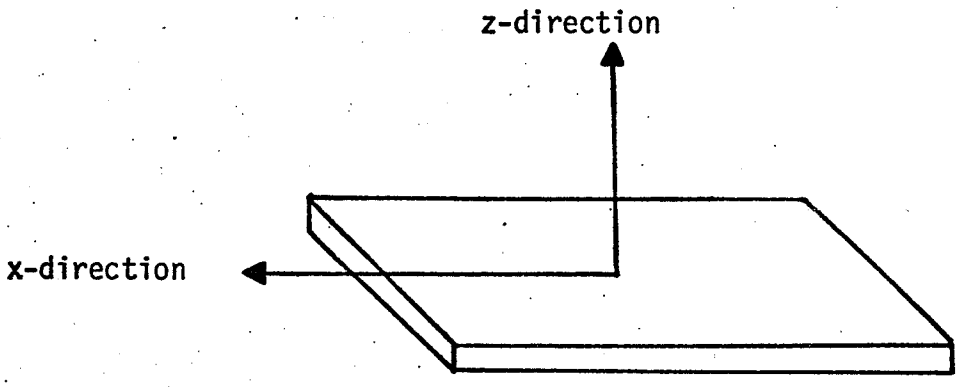

Fig. 4. Directions of measurement of lattice strain and total strain.

ε_x: Total strain measured in x-direction (the direction of the tensile axis).

e_z: Lattice strain measured in z-direction.

e_x: Lattice strain in x-direction (calculated using Poisson's ratio).

with cobalt $K\alpha_1$ and chromium $K\alpha_1$ radiations are given in Table 2.

TABLE 2.

Calculated values for reflection angles.

Reflection (hkl)	Interplanar spacing dA°	Bragg angle, degrees	
		$CoK\alpha_1$	$CrK\alpha_1$
(110)	2.0268	52.4	68.8
(200)	1.4332	77.2	106.0
(211)	1.1702	99.7	156.1
(220)	1.0134	123.9	--
(310)	0.9064	161.32	--
(222)	0.8275	--	--

The (211) and (310) reflections were chosen for investigation with $CrK\alpha_1$ and $CoK\alpha_1$ radiations respectively. The (222) reflection was very weak and therefore was not chosen for experimentation. Inverse-intensity measurements were carried out at known angular increments across the peak in consideration. The reflections from cementite were extremely weak to be of any significance.

In order to determine the interplanar spacings "d" to a precision adequate for the measurement of lattice strain, the 2θ angles of the diffracted rays have to be measured accurately. Several workers[24,25,26] have tried to establish methods for accurate

determination of the peak positions. In Ogilvie's parabola fitting method[25], five data points are obtained at equal 2θ intervals about the diffraction peak, and the parabolic curve is fitted by the method of least squares. Koistinen and Marburger[26,28] greatly simplified the computation procedure and the operation took less time by reducing the number of data points to three. The important limitation of this method, hoever, is that it depends on the line symmetry, and special attention has been drawn to this fact by Werner[5].

If the three points recorded correspond to at least 85% of the maximum intensity and these points straddle the peak of the diffraction curve, some lack of symmetry can be tolerated and the parabola will usually be a good approximation.

A long-range continuous scan of each peak preceded the step-scanning procedure. This was done essentially to establish the range over which the peak was to be scanned step-wise.

The peak positions were determined by parabola fitting following Koristinen and Marburger.[26,28] According to this method, we have :

$$2\theta \text{ vertex} = 2\theta_1 + c\ [(3a + b)/(a + b)]$$

where $a = t_1 - t_2$

$b = t_3 - t_4$

t_1, t_2 and t_3 are the time required to accumulate given number of counts at $2\theta_1$, $2\theta_2$ and $2\theta_3$.

$2\theta_1$, $2\theta_2$ and $2\theta_3$ are the consecutive 2θ positions at which inverse intensities are measured; and $c = 2\theta_2 - 2\theta_1$ or $2\theta_3 - 2\theta_2$.

The limit of accuracy in measurements of the change in

interplanar spacing, Δd from line shifts was $\pm$ 1 x 10^{-5} A°. This was facilitated by the preparation of charts giving the values of d-spacings with corresponding 2θ angles ranging from 0° to 180° for both Co $K\alpha_1$ and Cr $K\alpha_1$ radiations through a program run on the computer. The total strain was measured, accurate to $\pm$ 1 x 10^{-6} with the help of a Budd Strain Indicator.

A study undertaken to observe the variation in the X-ray peak position with change in temperature revealed a variation of 0.005° [2θ] for a change of 1.75° in room-temperature during the day, which was negligible.

2.4.2. Pulse Height Discrimination and Fixed Count Operation

The apparatus used was a combination of Philips X-ray generator with a vertical goniometer and a step-scanning device with step-scanning control combination. The pulse height analyser fed the counter assembly, whose numerical output was fed in the form of number of seconds taken to count a fixed number of pulses, on the Digital Printer. The goniometer divergence slit was set to 1° and the receiving slit to 0.05°. The cobalt target was used with an applied voltage of 40 kv and a tube current of 20 ma., while the chromium target was used with an applied voltage of 35 kv and a tube current of 20 ma. Iron and vanadium filters were used for cobalt and chromium targets respectively in order to remove the Kβ components of the wavelengths. This was followed by a threshhold pulse height analysis to remove the longer wavelength components of the background, and a suitable window setting to pass the Kα component alone. The step-scanning device facilitated an automatic advancement of the

goniometer in steps of 0.01° from a chosen angle on the lower side of the reflection peak. At each step, the time taken for the passage of 20,000 X-ray pulses was measured. A range of about 0.5° [2θ] was scanned, which resulted in a set of 50 readings for each peak.

The choice of a constant count of 20,000 X-ray pulses was a result of the following consideration [29]. The accuracy of counting of the pulses is governed by the laws of probability and this is essentially due to the statistical nature of the arrival of X-ray quanta. This necessitates counting of the pulses to be spread out over a sufficient length of time. For N random counts, the probable error having a 50% probability is given by $0.6745/\sqrt{N}$ or $\frac{67\%}{\sqrt{N}}$. The probability that this error will be exceeded is only 0.04 if we use three times the probable error as the determining factor, i.e. 3 x probable error or $\frac{3 \times 67\%}{\sqrt{N}}$. In a total of 20,000 counts, there is a 96% probability of being within an error of $\frac{3 \times 67\%}{100\sqrt{2}} = 1.4\%$. Furthermore, it was found that, when operating on a per cent count, the error in the reading of the Digital Printer was 0.01 sec. $\pm$ 0.01% of the reading. In order to maintain the statistical error in the counter and the error in the Printer to the same approximate magnitude of 1%, it was decided to use a fixed count of 20,000 X-ray pulses.

2.4.3. X-ray Background Intensity Measurements

Continuous scanning of the peaks was done at a constant speed of 1/8° per minute with the time constant at four seconds. This operation was performed at predetermined steps as the specimens were being loaded at a uniform strain rate of 10^{-3} per minute. The background intensity was taken as a straight line drawn

between points on each side of the peak that appear to be uninfluenced by the peak in question or by any neighbouring peaks or by any absorption edges that abruptly alter background intensities [30]. Changes, if any, in the level of the background intensity were studied.

3. RESULTS AND DISCUSSION

3.1 Cyclic Variation of the Lattice Strain Beyond the Limit of Proportionality.

A standard tensile curve for a specimen deformed on the Instron tensile testing machine is represented in fig. 5. The strain was measured with a strain gauge to a resolution of 4×10^{-6} at a constant strain rate of 5×10^{-3} per minute. The elastic loading modulus is 26.5×10^{6} psi.

Typical plots of lattice strain and total strain vs stress during uniaxial loading and unloading on the tensometer-attachment to the X-ray diffractometer are shown in figs. 6 - 9 [corresponding data in Tables 3 - 6] for both (310) and (211) reflections. The lattice strain, e_x , in the direction of pulling is obtained by dividing the lattice strain e_z, normal to pulling, by Poisson's ratio [ν]. The value of Poisson's ratio used in each case is determined by comparing the plots of applied stress vs total strain and applied stress vs lattice strain. While the average value of Poisson's ratio is readily available for polycrystalline metal, it is known to depend[28] upon the reflecting plane, the wavelength of the X-rays used, the complex interactions between a given grain and its surroundings and perhaps the grain size and other microstructural variables. Therefore, Poisson's ratio was determined for each tensile test.

The elastic loading modulus of figs. 6 - 9 is slightly lower than that of fig. 5, but the significant difference lies in the strain region, 15×10^{-4} to 120×10^{-4}, where the Instron curve

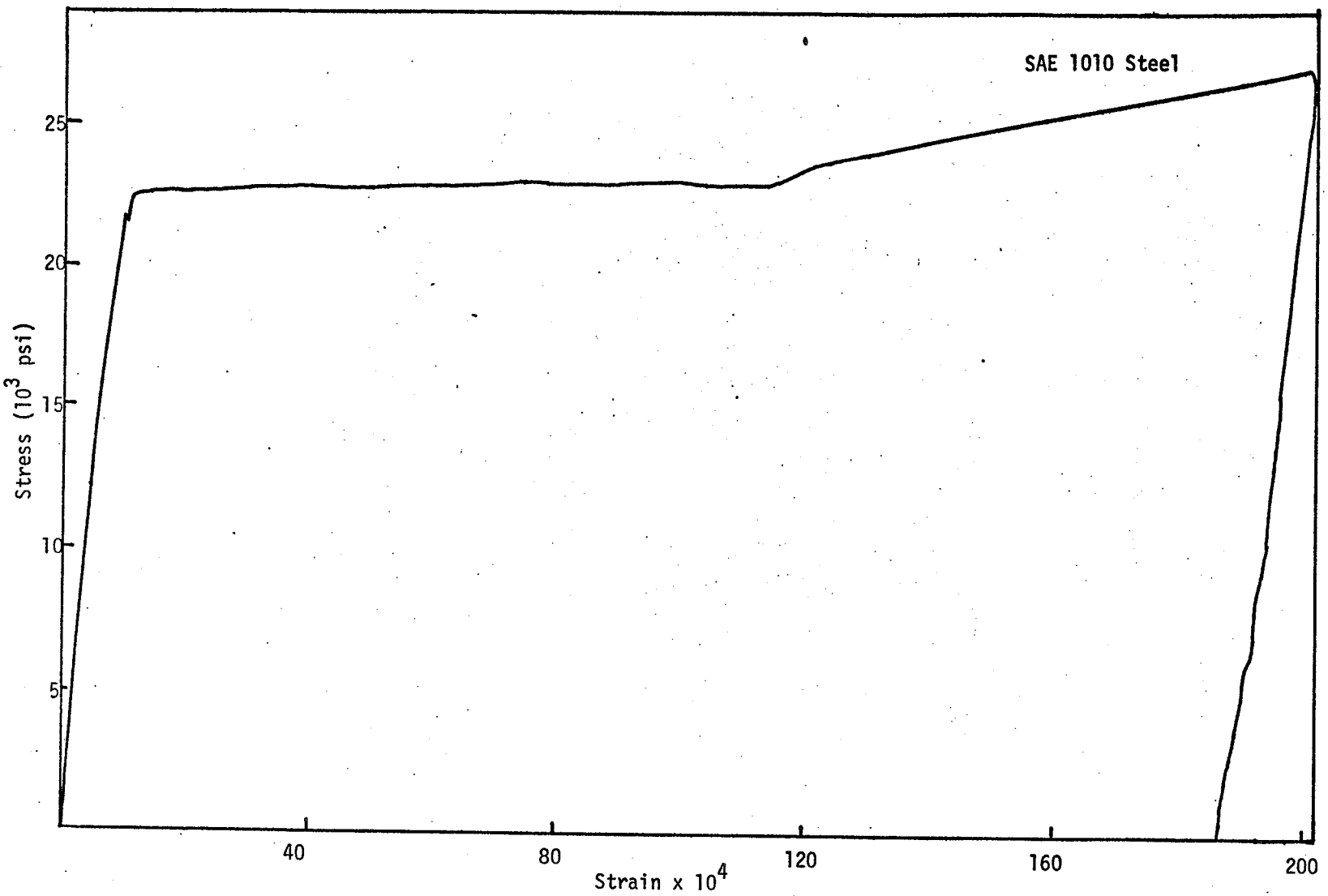

Fig. 5. Stress vs. strain plot obtained on the Inston Tensile Testing Machine.

TABLE 3.

SAE 1010 Steel: Specimen 6B

Line: (310)

Radiation: Co/Fe filter

Experimental Data:

No	Applied Stress, psi x 10^{-3}	Total Strain in direction of pulling, ε_x x 10^4 in/in	Lattice Strain, e_z normal to pulling, $\frac{\Delta d}{do}$ x 10^5	Lattice Strain, e_x in direction of pulling x 10^5	Remarks
1.	0	0	0	0	
2.	3.97	1.98	-5	+16	Poisson's Ratio $\nu = 0.32$
3.	7.95	3.87	-11	+34	
4.	11.92	5.54	-18	+55	
5.	13.91	7.14	-22	+69	
6.	15.90	11.82	-24	+76	
7.	17.88	36.47	-20	+62	
8.	19.87	66.93	-22	+69	
9.	21.86	96.42	-23	+72	
10.	23.85	121.33	-20	+62	
11.	0 (unloaded)	109.32	+15	-47	

Mode of Unloading: Instantaneous

Positive sign indicates expansion and negative sign indicates contraction in interplanar spacing.

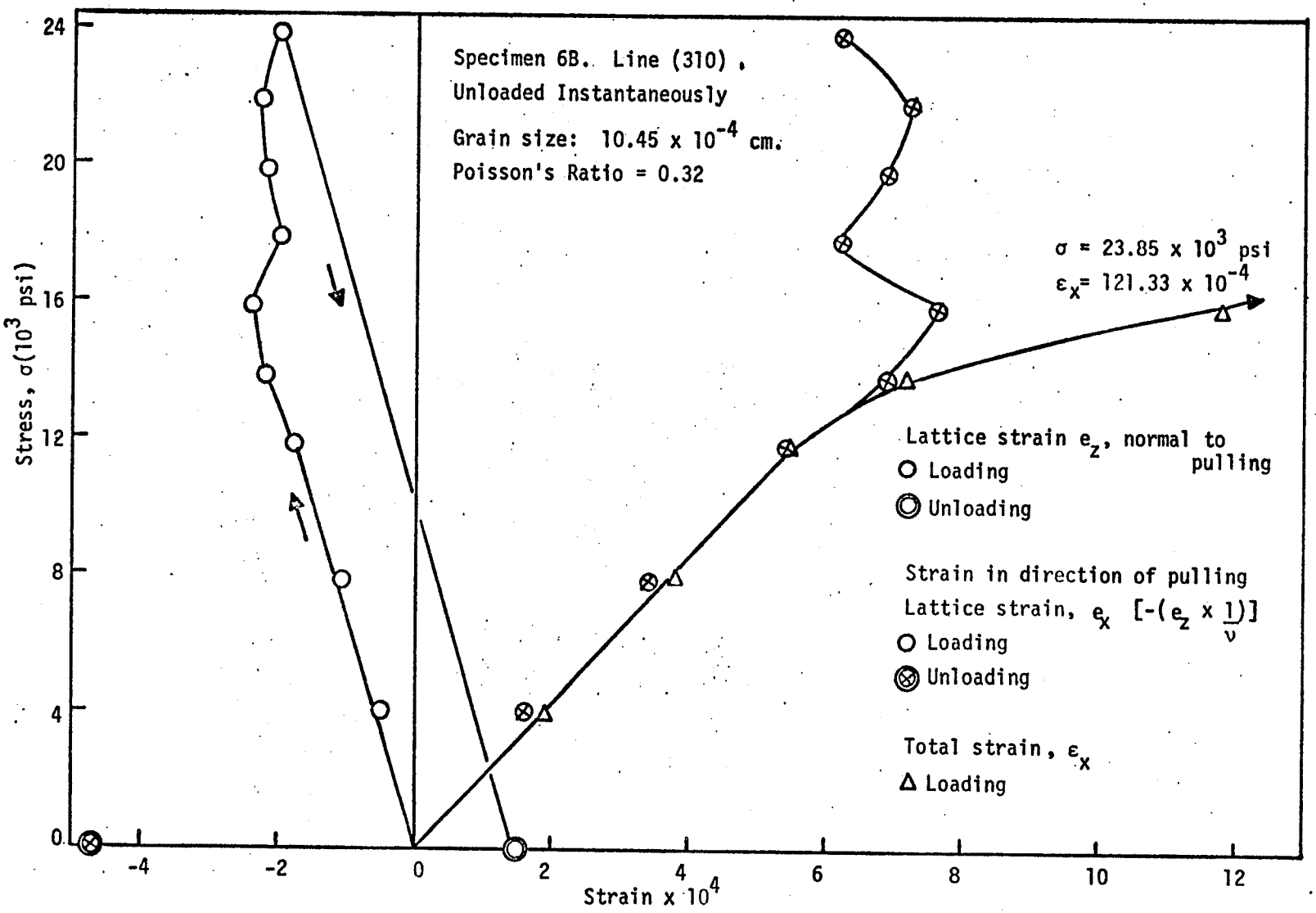

Fig. 6. Lattice strain and total strain vs. stress during uniaxial loading and unloading of SAE 1010 Steel.

TABLE 4.

SAE 1010 Steel: Specimen 9B.

Line: (211)

Radiation: Cr/V filter

Experimental Data:

No.	Applied Stress, psi x 10^{-3}	Total Strain in direction of pulling, ϵ_x x 10^4 in/in	Lattice Strain, e_z normal to pulling, $\frac{\Delta d}{do}$ x 10^5	Lattice Strain, e_x in direction of pulling x 10^5	Remarks
1.	0	0	0	0	
2.	4.85	2.06	-10	+22	
3.	9.7	4.18	-19	+41	Poisson's
4.	11.64	5.12	-21	+47	Ratio
5.	13.58	6.05	-26	+58	ν = 0.46
6.	15.51	7.67	-28	+62	
7.	17.45	29.36	-21	+45	
8.	19.39	54.32	-22	+49	
9.	21.33	87.96	-23	+50	
10.	23.27	114.23	-21	+45	
11.	0 (unloaded)	107.52	+15	-33	

Mode of Unloading: Instantaneous

Positive sign indicates expansion and negative sign indicates contraction in interplanar spacing.

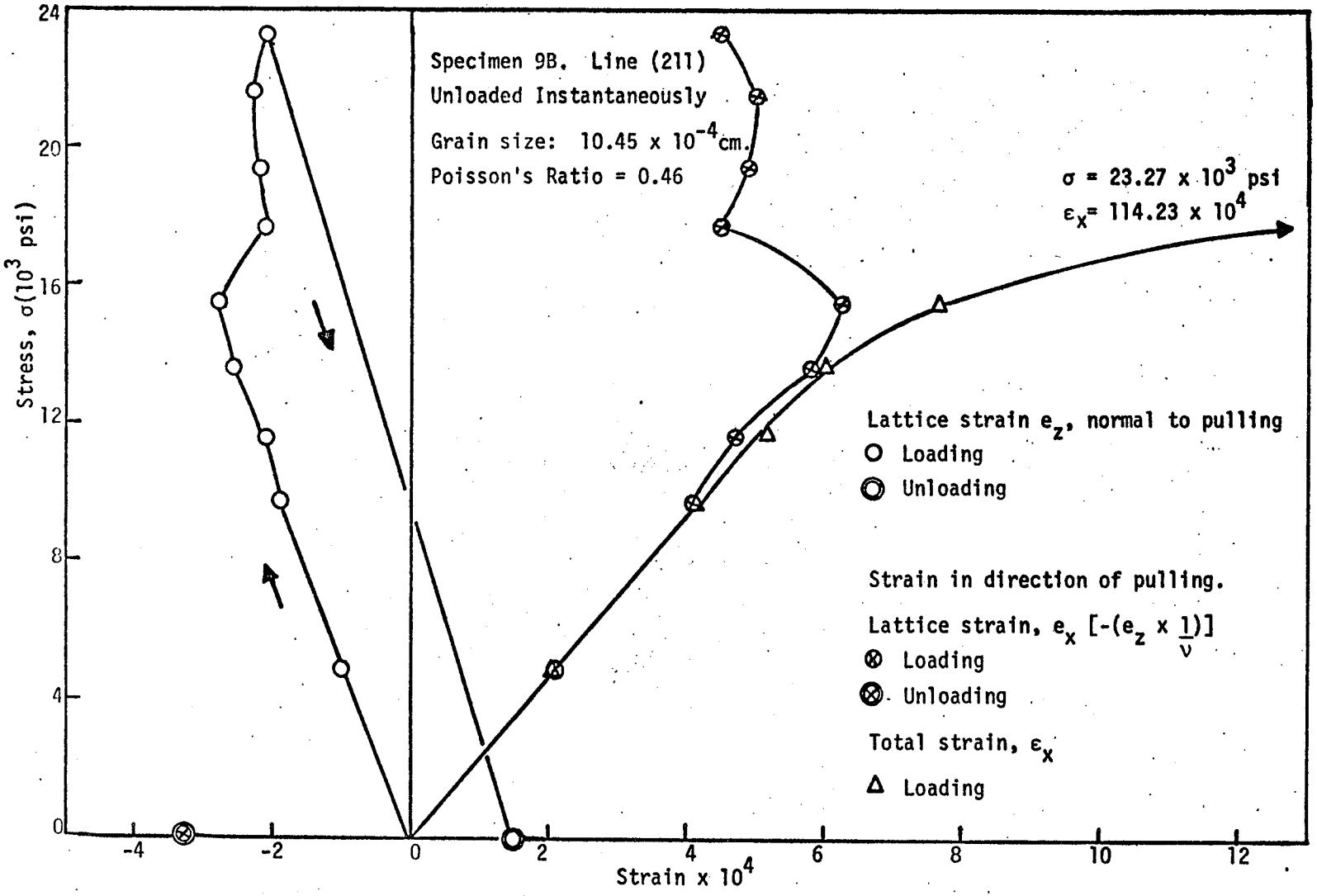

Fig. 7. Lattice strain and total strain vs. stress during uniaxial loading and unloading of SAE 1010 Steel.

TABLE 5.

SAE 1010 Steel: Specimen 11B.

Line: (211)

Radiation: Cr/V filter

Experimental Data:

No.	Applied Stress, psi x 10^{-3}	Total Strain in direction of pulling, ε_x x 10^4 in/in	Lattice Strain, e_z normal to pulling, $\frac{\Delta d}{do}$ x 10^5	Lattice Strain, e_x in direction of pulling x 10^5	Remarks
1.	0	0	0	0	
2.	4.67	2.05	-4	+18	
3.	9.34	4.1	-10	+43	Poisson's Ratio ν = 0.24
4.	14.0	8.12	-19	+78	
5.	16.34	13.8	-17	+71	
6.	18.67	46.52	-23	+96	
7.	21.0	86.5	-27	+110	
8.	23.34	126.58	-26	+107	

Mode of Unloading: Gradual

Positive sign indicates expansion and negative sign indicates contraction on interplanar spacing.

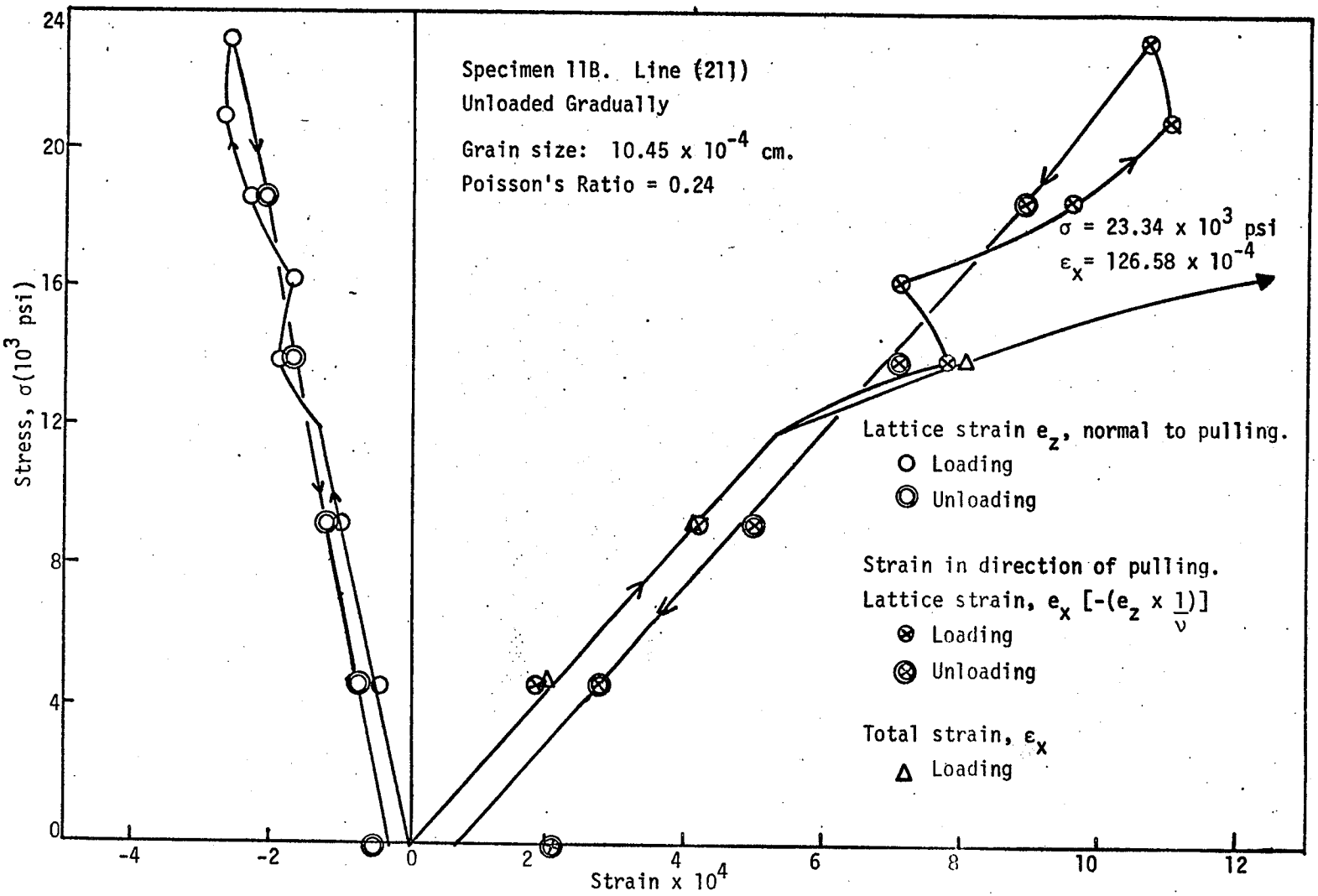

Fig. 8. Lattice strain and total strain vs. stress during uniaxial loading and unloading of SAE 1010 Steel.

TABLE 6.

SAE 1010 Steel: Specimen 13B.

Line: (310)

Radiation: Co/Fe filter

Experimental Data:

No.	Applied Stress, psi x 10^{-3}	Total Strain in direction of pulling, ε_x x 10^4 in/in	Lattice Strain, e_z normal to pulling, $\frac{\Delta d}{do}$ x 10^5	Lattice Strain, e_x in direction of pulling x 10^5	Remarks
1.	0	0	0	0	
2.	3.86	1.83	-6	+16	
3.	7.71	3.68	-13	+38	
4.	11.57	5.42	-19	+54	Poisson's
5.	13.49	7.23	-23	+66	Ratio
6.	15.42	12.34	-30	+85	ν = 0.35
7.	17.35	38.47	-25	+73	
8.	19.28	58.36	-28	+79	
9.	21.20	97.73	-29	+82	
10.	23.13	113.25	-25	+73	

Mode of Unloading: Gradual

Positive sign indicates expansion and negative sign indicates contraction in interplanar spacing.

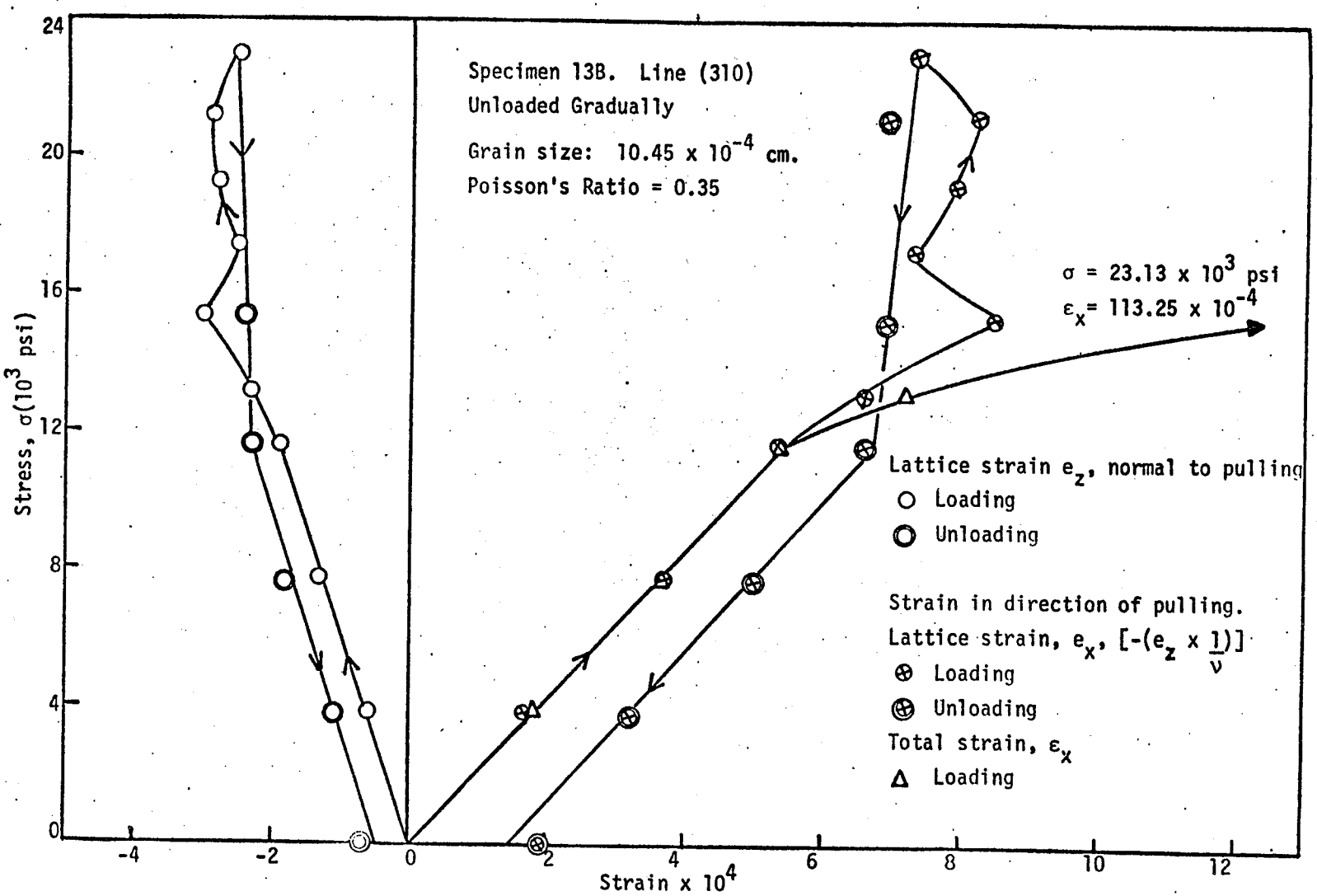

Fig. 9. Lattice strain and total strain vs. stress during uniaxial loading and unloading of SAE 1010 Steel.

shows no work hardening. This could be due to the intermittent loading on the tensometer-attachment to the X-ray diffractometer unlike the continuous loading on the Instron tensile testing machine.

Fig. 10 schematically illustrates the salient features of figs. 6 - 9, which can be summarised as follows: The lattice strain measured by X-rays as well as the total strain measured by strain indicator are proportional to the stress up to about 12×10^3 psi. Thereafter,the lattice strain first increases at an increasing rate [corresponding to BC] and then decreases [corresponding to CD]. Subsequently, it is seen to increase once again at an increasing rate [DE] only to be followed by a decrease [EF]. In other words, this phenomenon appears to be cyclic in nature and is probably due to inhomogeneous deformation processes.

Recently, Orlov[31] has shown that heterogeneous deformation occurs within the yield plateau of annealed iron specimens. The specimens were 50 mm. long, 4 mm. wide and 0.1 mm. thick with a mean ferritic grain size of 50-60μ and were deformed at an elongation rate of 3 mm/minute. Orlov found that the end of the yield plateau [which essentially depends on the grain size, dimensions of the specimen, etc.] corresponds to an average elongation of 6%.

The possible mechanisms for such a heterogeneous deformation are as follows:

(a) Sources of dislocations might give rise to localized deformation within the grains.

Various sources of dislocations have been identified in the very early stages of deformation in polycrystalline metals. For example, Singh and Tangri[32] show evidence for dislocation sources

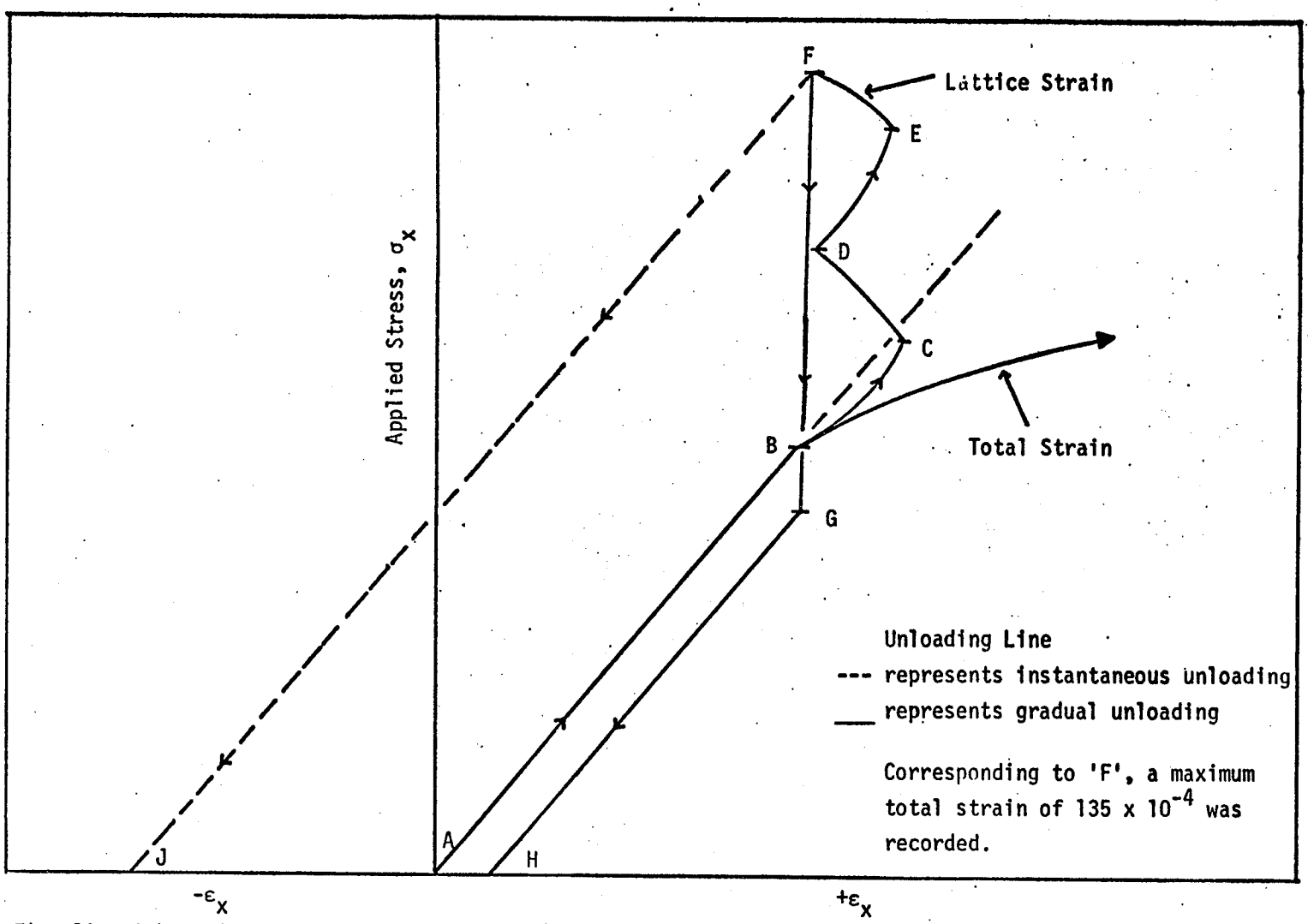

Fig. 10. Schematic variation of the strain (total and lattice) and the applied stress in the x-direction.

operating at twin and grain boundaries in polycrystalline nickel. Brandon and Nutting[33] suggest a possibility of the grain boundaries acting as a reservoir of dislocations. Under the influence of an applied stress, dislocations emerge and cause deformation. The mechanisms by which grain boundaries act as sources of dislocations have also been described by Bäro et al[34].

(b) Some suitably oriented segments of the dislocation network might get activated. Such a generation of dislocations could occur by the Frank-Read mechanism.

Mitchell and Smialek[35] have shown that $\frac{\tau_c L}{Gb}$ [where τ_c = critical stress for a Frank-Read source, L = source length, G = shear modulus and b = burgers vector] varies with L/b and such a variation is seen to depend on the character of the dislocation.

Assuming that:

$\tau_c = 1.2 \times 10^3$ psi [≃limit of proportionality]

$G = 11 \times 10^6$ psi

then $\frac{L}{b} = 1100$ [for an edge source]

hence if $b = 2.5 \times 10^{-8}$ cm.

we have $L = 1100 \times 2.5 \times 10^{-8}$ cm.

$= 2.75 \times 10^{-5}$ cm.

The above quantity which is very small in comparison with the grain size of the specimens under investigation, is indicative of the ease of operation of an edge source.

(c) Only those grains of the experimental specimen will deform plastically where the resolved shear stress on the slip plane in the slip direction reaches a constant critical value corresponding to

$$\tau_{max.} = 0.5\ \sigma_t$$

Here, $\tau_{max.}$ = maximum resolved shear stress

σ_t = tensile stress

and the constant, 0.5, is the maximum value of the Schmid factor.

(d) The observations of Orlov[31] suggest an avalanche-type propagation of plastic flow associated with the rapid multiplication of dislocations on the "line" of the advancing deformation front. It is interesting to note that in the present study the end of the concomitant yield plateau corresponds to about 1.3% as shown in fig. 5.

All the four of the above mentioned mechanisms could be contributory to the heterogeneous deformation. Thus, the observed cyclic variation in the stress vs lattice strain plot [schematic fig. 10] may be explained as follows:

BC in fig. 10: There is a delay in the mass multiplication of dislocations. Depending on orientation, an increase in stress might be necessary before slip starts to occur in some of the grains. It is also likely that slip might have been activated in some other grains of high Schmid factor. There is an increase in the lattice strain in stage BC as seen in the proportional elastic region. This means that the overall effect is continuation of the elastic bahavior.

CD in fig. 10: At C, a number of sources of dislocations might be activated in a large number of grains. An accelerated multiplication of dislocation by avalanche-type flow occurs resulting in a relaxation in the matrix. The consequent decrease in the lattice strain is shown by the reversal of CD.

DE in fig. 10: Fewer sources of dislocations might be available as a result of exhaustion of the sources that were active

earlier. While some dislocation segments might have been rendered free in stage CD, there could be some other segments which are difficult to activate due to their orientation, length, etc. A build-up of stress might be necessary before a subsequent rapid multiplication of dislocations takes place in a narrow zone of the 'line' of the deformation front. Once the relaxation of stage CD has taken place, normal elastic bahavior of the matrix is resumed giving rise to stage DE. It may be significant that DE [and BC] extends over a greater stress increment than CD which suggests that the relaxation is rather a sudden process as is the production of an avalanche of dislocations. Before another such avalanche occurs, significant stress increment must be applied.

EF in fig. 10: Again at a higher stress, further plastic flow similar to that in the region CD occurs with a corresponding relaxation reflected by a decrease in the interplanar spacing.

Similar cyclic variations of the lattice strain are seen to occur for (310) as well as (211) planes, but the actual stress values corresponding to B, C, D, etc. are different.

Since such processes occur in localized regions, the effects are seen only in the stress vs lattice strain plot and a recording instrument of high sensitivity might be required to observe corresponding effects of stress vs total strain.

While the proposed hypothesis offers a tentative explanation for the cyclic variation of the lattice strain, electron microscopic evidence is needed to arrive at definite conclusions.

3.2 The Behavior of the Lattice [Elastic] Strains During and Subsequent to Unloading.

Cullity[19] has prepared a schematic summary of the results of previous workers, mainly Smith and Wood, which suggests that above the elastic limit the lattice strain may increase, or may even decrease with increase in applied stress. If the applied stress is then decreased, the lattice strain should decrease along a line parallel to the loading line in the elastic region and thus produce a compressive residual lattice strain after unloading. However, depending upon the mode of unloading[22], both compressive and tensile strains have been observed in nickel deformed up to 0.29% strain. Therefore, an attempt was made to study the behavior of lattice strains during and subsequent to unloading in low carbon steel deformed up to 1.35% strain.

Specimens Unloaded Instantaneously.

Plots of lattice strain and total strain against stress during uniaxial loading and instantaneous unloading of low carbon steel are shown in figures 6 and 7 and the data are found in Tables 3 and 4.

On unloading the specimens instantaneously from a stress level above the macroscopic limit of proportionality, an anelastic recovery [about 0.3×10^{-4} in./in] of the total strain [ε_x] is seen to occur, which can be reasonably expected.

The residual lattice strain subsequent to instantaneous unloading is found to be tensile in a direction perpendicular to that of pulling [e_z]. On aging at room temperature, this reverses to a residual compressive lattice strain [Tables 7 and 8].

TABLE 7.

SAE 1010 Steel: Specimen 6B.

Line: (310)

Room Temperature Aging Data:

No.	Time in hours	Total Strain in direction of pulling, $\varepsilon_x \times 10^4$ in/in	Lattice Strain, e_z normal to pulling $\times 10^5$
1.	0	109.32	15(+)
2.	2	109.24	13(+)
3.	12	109.16	1(+)
4.	61	109.03	1(+)
5.	62	109.03	0
6.	63	109.03	0

Mode of Unloading: Instantaneous

e_z: Positive sign indicates expansion and negative sign indicates contraction in interplanar spacing.

TABLE 8.

SAE 1010 Steel: Specimen 9B.

Line: (311)

Room Temperature Aging Data:

No.	Time in hours	Total Strain in direction of pulling, $\epsilon_x \times 10^4$ in/in	Lattice Strain, e_z normal to pulling $\times 10^5$
1.	0	107.52	15(+)
2.	1.5	107.41	11(+)
3.	3	107.29	0
4.	5	107.24	0
5.	8	107.23	1(-)
6.	20	107.22	1(-)
7.	25	107.22	1(-)

Mode of Unloading: Instantaneous

e_z: Positive sign indicates expansion and negative sign indicates contraction in interplanar spacing.

Several specimens have been loaded to various stress levels and instantaneously unloaded. The lowest stress level which gave rise to a residual lattice strain was 12.08×10^3 psi [at a corresponding total strain of 5.22×10^{-4} in/in] which is equivalent to the limit of proportionality. The results corresponding to various specimens loaded to predetermined values of stress [and instantaneously unloaded] are shown in Table 9. Each specimen has been aged for 22 hours at room temperature subsequent to instantaneous unloading, and the reversal in the residual lattice strain [RLS] has been determined. A plot of the reversal in the RLS against prior plastic strain is shown in fig. 12.

Specimens Unloaded Gradually.

Plots of lattice strain and total strain against stress during uniaxial loading and gradual unloading of low carbon steel are shown in figs. 8 and 9 and the data are found in Tables 5, 6, 10, and 11.

The anelastic recovery [about 0.1×10^{-4} in/in] of the total strain subsequent to gradual unloading over a period of about 12 hours is much less than that following instantaneous unloading. This is attributed to the fact that part of the anelastic recovery occurs during the process of gradual unloading.

The residual lattice strain subsequent to gradual unloading is found to be compressive in a direction perpendicular to that of pulling [e_z]. No significant change is seen to occur in the residual lattice strain on aging at room temperature [Tables 12 and 13].

TABLE 9.

SAE 1010 Steel: Effect of Room Temperature Aging on RLS in Specimens Instantaneously Unloaded Subsequent to Varying Amounts of Deformation in Uniaxial Tension

Line: (310)

Radiation: Co/Fe filter

Ser. No.	Spec. No.	Prior Plastic Strain in direction of pulling x 10^4 in/in	RLS, e_z normal to pulling (immediately after unloading) x 10^5	RLS, e_z' normal to pulling (after aging for 22 hrs.) x 10^5	Reversal in RLS $R=(e_z'-e_z) \times 10^5$
1.	14B'	-	+1	0	1
2.	15B'	0.3	+9	+7	2
3.	16B'	2.56	+2	-1	3
4.	17B'	19.92	+4	-3	7
5.	18B'	35.91	+6	-4	10
6.	19B'	61.51	+10	-3	13
7.	20B'	80.43	+10	-3	13
8.	6B	110.83	+15	0	15

RLS: Residual Lattice Strain

Positive sign indicates expansion and negative sign indicates contraction in interplanar spacing.

TABLE 10.

SAE 1010 Steel: Specimen 11B.

Line: (211)

Data on Gradual Unloading:

No.	Applied Stress, psi x 10^{-3}	Total Strain in direction of pulling $\epsilon_x \times 10^4$ in/in	Lattice Strain, e_z normal to pulling $\frac{\Delta d}{do} \times 10^5$ (-)	Lattice Strain, e_x in direction of pulling x 10^5 (+)
1.	18.67	124.94	21	89
2.	14	122.48	17	71
3.	9.34	120.42	12	50
4.	4.67	117.46	7	28
5.	0	116.28	5	21

TABLE 11.

SAE 1010 Steel: Specimen 13B

Line: (310)

Data on Gradual Unloading:

No.	Applied Stress, psi x 10^{-3}	Total Strain in direction of pulling ϵ_x x 10^4 in/in	Lattice Strain, e_z normal to pulling $\frac{\Delta d}{do}$ x 10^5 (-)	Lattice Strain, e_x in direction of pulling x 10^5 (+)
1.	19.28	110.68	24	69
2.	15.42	109.83	24	69
3.	11.57	108.65	23	66
4.	7.71	105.06	18	50
5.	3.86	103.64	11	32
6.	0	100.27	7	19

TABLE 12.

SAE 1010 Steel: Specimen 11B.

Line: (211)

Room Temperature Aging Data:

No.	Time in hours	Total Strain in direction of pulling, $\epsilon_x \times 10^4$ in/in	Lattice Strain, e_z normal to pulling $\times 10^5$ (-)
1.	0	116.28	5
2.	3	116.24	4
3.	4	116.19	5
4.	12.75	116.06	5
5.	14.5	116.04	5
6.	15.5	116.02	4
7.	16.5	116.02	4

Mode of Unloading: Gradual

e_z: Positive sign indicates expansion and negative sign indicates contraction in interplanar spacing.

TABLE 13.

SAE 1010 Steel: Specimen 13B.

Line: (310)

Room Temperature Aging Data:

No.	Time in hours	Total Strain in direction of pulling, $\epsilon_x \times 10^4$ in/in	Lattice Strain, e_z normal to pulling $\times 10^5$ (-)
1.	0	100.27	7
2.	1.5	100.23	6
3.	3	100.18	7
4.	5	100.11	5
5.	8	100.08	5
6.	20	100.07	5
7.	25	100.07	5

Mode of Unloading: Gradual

e_z: Positive sign indicates expansion and negative sign indicates contraction in interplanar spacing.

There are significant observations which are contrary to the predictions of Cullity's hypothesis[19] [fig. 11]:

(a) At higher stresses, a cyclic variation in the lattice strain with applied stress [Section 3.1] has been observed.

(b) Depending on the mode of unloading, both compressive and tensile residual lattice strains have been observed. The values of the lattice strains e_x corresponding to points obtained during gradual unloading are all tensile in nature; and the residual lattice strain, e_x, obtained is also tensile.

Regardless of the sign of the residual stress which is detected by X-rays from the coherently diffracting regions and as such from the bulk of the material, a balancing stress of opposite sign must also be present in some non-coherently diffracting regions. It is suggested, following Newton[36] and Cullity[1], that these regions of opposing stress are the dislocation substructures produced during deformation rather than the previously existing grain boundaries.

The observed residual tensile strain, e_z, after instantaneous unloading and its gradual reversal to a compressive strain with time may be explained by the mechanism proposed by Swaroop and Tangri[22]. It is well established[37,38,39] that a non-equilibrium distribution of point defects is produced during the deformation of a metal. This is expected to cause a general expansion of the lattice. Assuming that the effect of instantaneous unloading is analogous to that of quenching, a net tensile strain e_z, as experimentally observed, may be expected if the general expansion resulting from the presence of point defects in the lattice is more than the compressive strain due to the stress system developed by the substructure walls and the

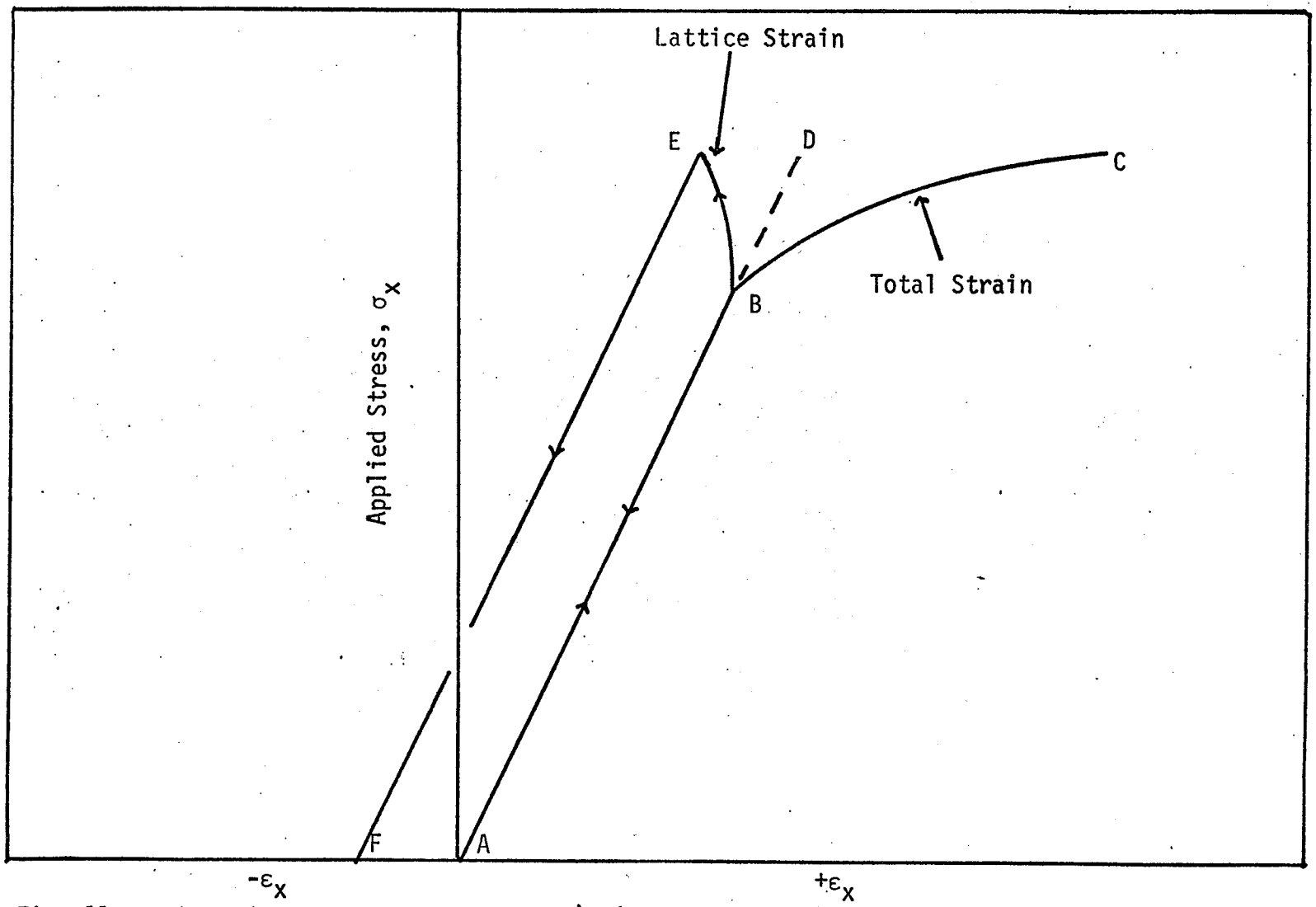

Fig. 11. Schematic variation of the strain (total and lattice) and the applied stress in the x-direction. (B.D. Cullity, 1963)

matrix. Therefore, on subsequent aging at room temperature, the expansion of the lattice will progressively decrease until a compressive strain similar to that observed during the gradual unloading of a specimen [in 6 to 12 hours] is observed.

While it is accepted that vacancies are produced by cold work, we still do not know the relation between the number produced and the plastic strain. Seitz[40] and Mott[41] suggested that a plastic strain ε_p produces a concentration, c, of vacancies given in the order of magnitude by:

$$c \simeq 10^{-4} \varepsilon_p \qquad \text{Eqn. 3.2.1.}$$

Semiquantitative estimates[47] indicate that the atomic fraction of defects produced by the geometric mode of generation is proportional to the plastic strain with a proportionality constant of 10^{-4} to 10^{-5}. However, van Bueren and Jongenburger[42] have shown the resistivity change, $\frac{\Delta\rho}{\rho}$ with elongation $\frac{\Delta l}{l}$ as

$$\frac{\Delta\rho}{\rho} \simeq \frac{\Delta l}{l}^{3/2} \qquad \text{Eqn. 3.2.2.}$$

the proportionality factor being of the order of unity. Van Bueren[42] has connected this observation with a theory in which expanding dislocation rings develop jogs on themselves at a rate proportional to the area of slip plane swept by the rings, and in which these jogs produce point defects at a rate proportional to the distance they move through the slip plane. Thus, the concentration of point defects is expected to vary as:

$$c \propto \varepsilon_p^{3/2} \qquad \text{Eqn. 3.2.3.}$$

Several mechanisms[40] have been proposed for the production of point defects. Until recently, a generally accepted process has

been the intersection of two screw dislocations, leading to the formation of a jog capable of producing point defects by moving with the screw. Friedel[43] considers that the two arms of a Frank-Read source may often lie in neighbouring glide planes when they coalesce at the end of each cycle of operation of the source. A line of point defects is thus formed, the number of which is of the order of l/b, where l is the length of the source and b is the atomic spacing. Each time the source operates, l/b defects are created, so that the concentration c produced by N cycles of operation per unit volume is given by:

$$c \simeq (l/b)\, vN, \qquad \text{Eqn. 3.2.4.}$$

where $v(\simeq b^3)$ is the atomic volume. If the area swept by each dislocation ring is L^2, the plastic strain is given by $\varepsilon_p = L^2\, bN$; hence:

$$c \simeq (lb/L^2)\, \varepsilon_p. \qquad \text{Eqn. 3.2.5.}$$

Assuming that $L \simeq 3xl = 3 \times 10^4\, b$, this gives

$$c \simeq 10^{-5}\, \varepsilon_p. \qquad \text{Eqn. 3.2.6.}$$

A plot of the reversal in the RLS vs prior plastic strain is shown in fig. 12. In order to find a power law, the above data was plotted on a log-log scale [fig. 13]. The best fit straight line through these points gave the following relation between the reversal in the RLS, R and the prior plastic strain, ε_p.

$$R = 1.11 \times 10^{-3}\, \varepsilon_p^{0.445}$$
$$\simeq 1.11 \times 10^{-3}\, \varepsilon_p^{1/2} \qquad \text{Eqn. 3.2.7.}$$

The disagreement between the above equation and that due to Seitz[40] and Mott[41] indicates that the reversal in the RLS subsequent to instantaneous unloading is not entirely due to the annihilation of vacancies.

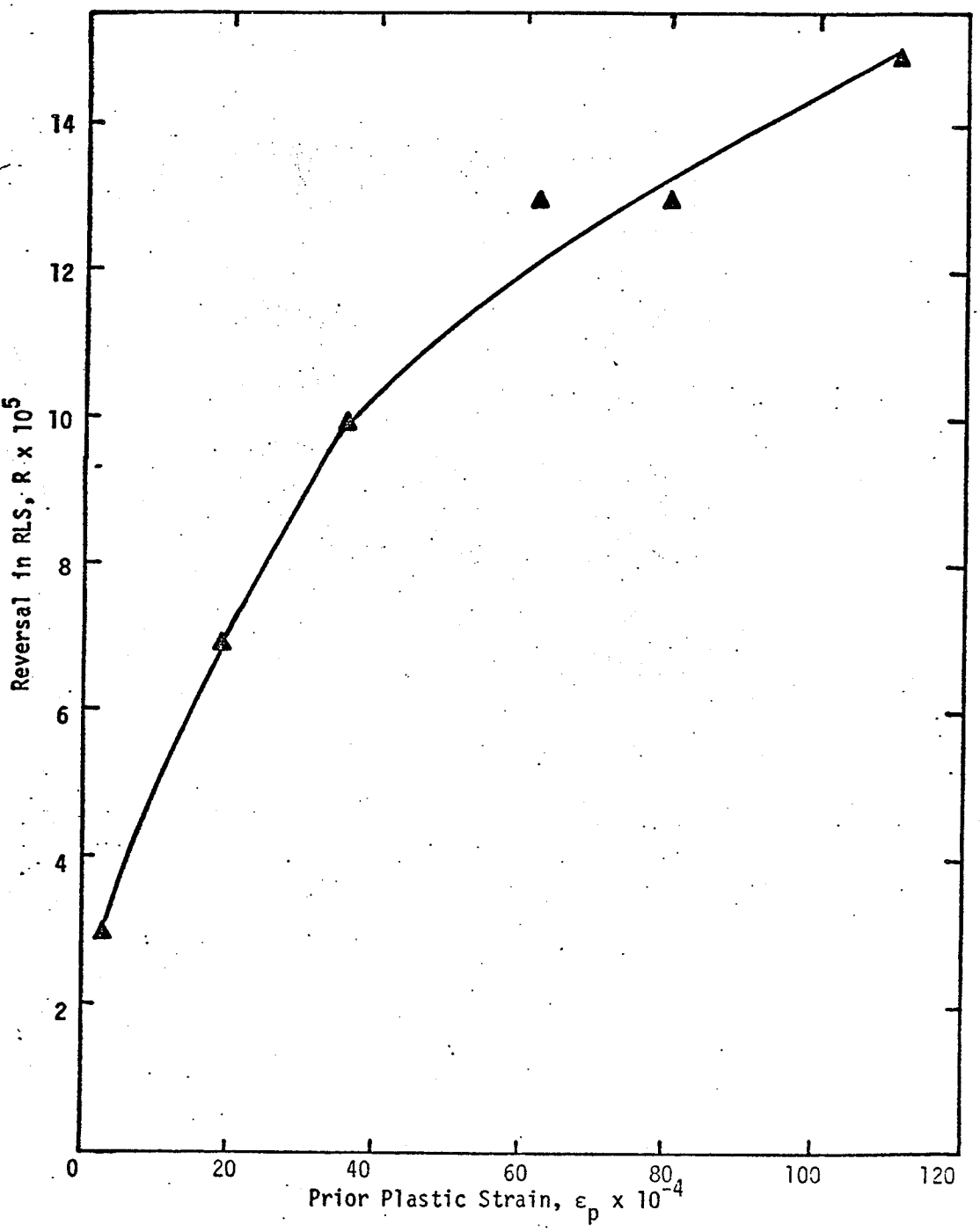

Fig. 12. Plot of the reversal in RLS vs. prior plastic strain.

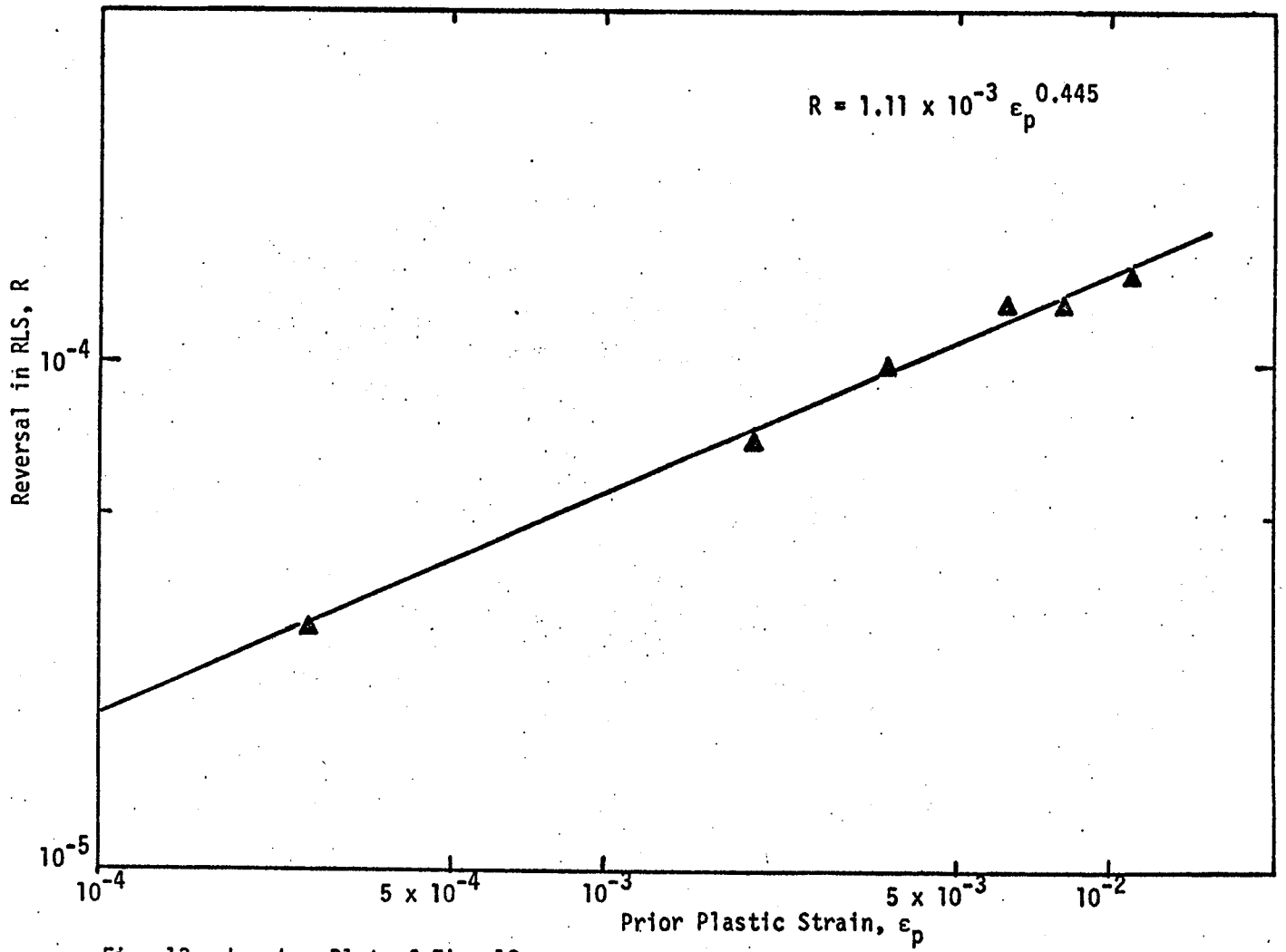

Fig. 13. Log-Log Plot of Fig. 12.

The atom fraction of point defects, n can be found by the following relation[45]:

$$\frac{\Delta a}{a} = \frac{1}{3}\,\frac{Vx}{Vo}\,n. \qquad \text{Eqn. 3.2.8.}$$

where $\frac{\Delta a}{a}$ is equivalent to $\frac{\Delta d}{d}$, Vx is the volume change produced by the strains of one defect and Vo is the atomic volume of the perfect crystal. The average value of $\frac{\Delta d}{do}$ for instantaneously unloaded specimens [deformed to a plastic strain of about 1%] is found to be 15×10^{-5} [reflection: 310]. Assuming[46] that

$$\frac{Vx}{Vo} = 0.5,$$

the value of n obtained is of the order of 10^{-3} atomic fraction. This differs from semiquantitative estimates[47] by 2 to 3 orders of magnitude.

For a plastic strain of 1%, we should have, according to Seitz[40] and Mott[41], only 10^{-6} vacancies. However, we need 10^{-3} vacancies according to Eqn 3.2.7. This could be due to the fact that the RLS in the instantaneously unloaded specimen must be due to both the production of vacancies and dislocation substructure. Since the magnitude of reversal in the RLS is approximately of the same order of magnitude as the RLS in an instantaneously unloaded specimen, the causes of RLS are intimately associated with those of the reversal in the RLS. The reversal in the RLS of the instantaneously unloaded specimen from tension to compression [e_z] with room temperature aging can be attributed to both the annihilation of vacancies and the rearrangement of dislocations [anelastic effect].

3.3 The Variation of the X-ray Background Instensity with Deformation.

The contribution to the integrated intensity is from the coherently scattering domains of polycrystalline aggregate, while the background intensity is due to the incoherently scattering domains, for example, the grain boundaries or tangles of dislocations.

Dislocation tangles as well as clusters have been found to characterize metallic specimens even after a very small deformation. Several such observations have been made in nickel[32,49], iron[48,51,52] and niobium[50]. In iron, it has been found that once the clusters of dislocations are formed, with further deformation they become denser and closer together and tend to form a continuous network dividing the metal into separate cells.

In view of the above, a study of background intensity with deformation was undertaken. About ten specimens were deformed to 1.25% strain in gradual steps and unloaded gradually as well as instantaneously. At every step, continuous scanning of the peaks in question as well as background was done. The background intensity did not show any significant variation [even after deformation to strain values of 10%, 12%, 15% and 20%].

The background intensity of cold-worked metals has been examined by several workers with conflicting results. In particular, Averbach and Warren[53] have concluded that, for both brass and aluminium, the background intensities from severely cold-worked and annealed samples are identical to an accuracy of 2%, whereas Hall and Williamson[54] have reported a 15% increase on cold-working.

Calculations show that, for a grain size of 10.45×10^{-4} cm., only 0.0006% of a total volume of $1cm^3$ constitute the grain boundary

region [identical values were obtained for spherical as well as cubical grains]. The contribution to the background intensity is therefore expected to be very little, and hence any change in it cannot be observed without ambiguity.

3.4 Stacking Faults and Intergranular Stresses.

Shifts in the positions of X-ray lines have been found to occur with plastic deformation; and these have been attributed to changes in lattice parameter, to stacking faults[55], and to stress systems within the specimen[5]. A study of the shifts in the X-ray peak positions with uniaxial deformation was undertaken with a view to examine the possibilities mentioned above.

We have from the Bragg Equation,

$$\frac{\Delta d}{d} = -(\cot \theta)\, \Delta\theta.$$

For a uniform strain in the lattice, we can write $k \tan \theta = \Delta(2\theta)$, where k is a constant.

The positions of (110), (200), (211), (220) and (310) reflections have been determined for polycrystalline low carbon steel specimens in the annealed state. Thereafter, the specimens were uniaxially deformed to strains well beyond the limit of proportionality. The positions of the reflections mentioned above were determined subsequent to gradual as well as instantaneous unloading of specimens. The results are found in Tables 14 and 15. Plots of the shifts in the positions of Bragg maxima subsequent to deformation, $\Delta(2\theta)$ as a function of $\tan \theta$ are shown in figures 14 and 15.

It is well known that the geometry of the Norleco diffractometer is such that only planes parallel to the surface of the specimen [i.e. planes perpendicular to the tensile axis] contribute to the reflections measured. Therefore, it should be expected that the plot of $\Delta(2\theta)$ against $\tan \theta$ should yield a straight line if there is a uniform change in the lattice parameter due to the presence of a macroscopic stress on the material.

TABLE 14.

SAE 1010 Steel: Specimen 17B.

Angular Shifts in the Positions of X-ray Diffraction Lines, $\Delta(2\theta)$

Due to Uniaxial Loading and Unloading.

Mode of Unloading: Instantaneous

Bragg angle, Normal to pulling	(310)	(220)	(211)	(200)	(110)
2θ initial	161.205	123.87	99.67	77.185	52.33
2θ unloaded	161.16	123.845	99.66	77.178	52.33
$\Delta(2\theta)$	0.045	0.025	0.01	0.007	-
tan θ	6.04	1.87	1.18	0.80	0.49

Max. Applied Stress: 19.32×10^3 psi

Max. Total Elongation: 0.94%

Residual Total Strain: 51.41×10^{-4} in/in.

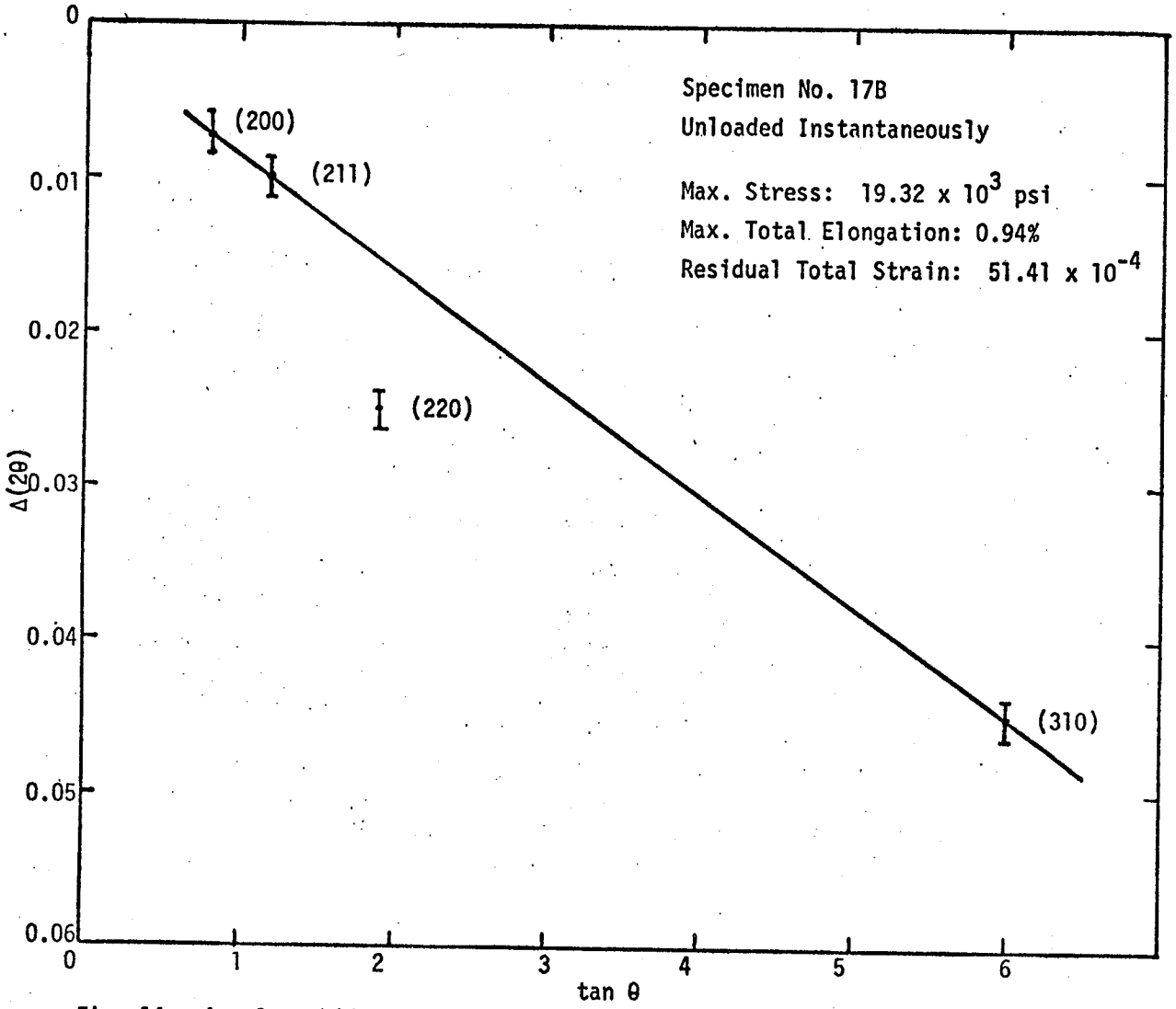

Fig. 14. Angular shifts in the positions of X-ray diffraction lines $\Delta(2\theta)$ as a function of tan θ.

TABLE 15.

SAE 1010 Steel: Specimen 19B.

Angular Shifts in the Positions of X-ray Diffraction Lines, $\Delta(2\theta)$

Due to Uniaxial Loading and Unloading.

Mode of Unloading: Gradual

Bragg angle, Normal to pulling	(310)	(220)	(211)	(200)	(110)
2θ initial	161.19	123.81	99.625	77.09	52.321
2θ unloaded	161.215	123.815	99.63	77.094	52.322
$\Delta(2\theta)$	0.025	0.005	0.005	0.004	0.001
tan θ	5.976	1.87	1.18	0.80	0.49

Max. Applied Stress: 15.59×10^3 psi

Max. Total Elongation: 0.56%

Residual Total Strain: 44.87×10^{-4} in/in.

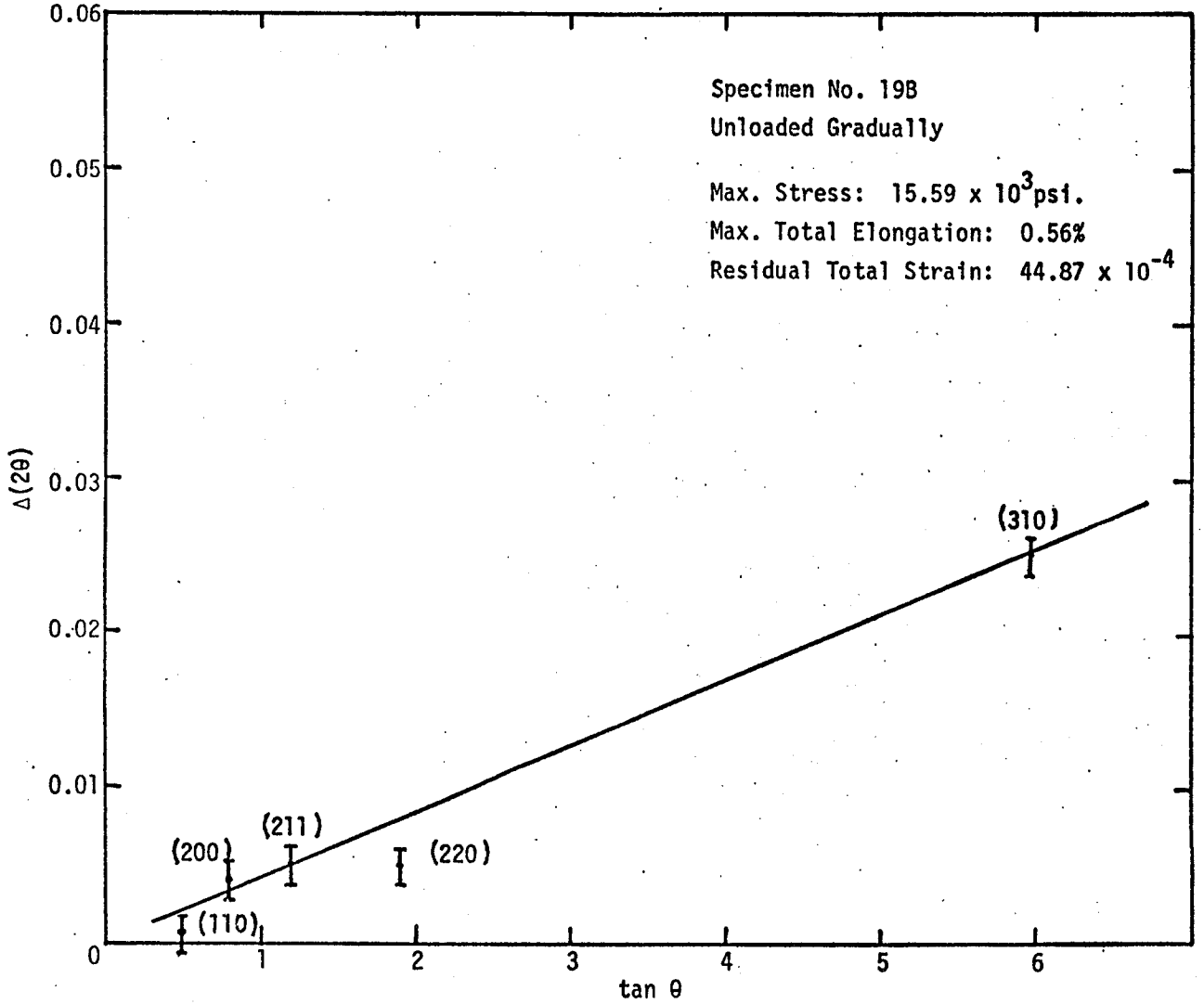

Fig. 15. Angular shifts in the positions of X-ray diffraction lines $\Delta(2\theta)$ as a function of tan θ.

Mitchell and Smith[56] have made measurements on gold and they find that with the exception of one weak reflection, there is no significant departure from a straight line and they attribute this to the low stacking fault probability and absence of intergranular stresses.

It is seen that for the instantaneously unloaded specimen, as well as the gradually unloaded specimen, the shifts are either all positive or all negative. The plots are almost linear with no significant departure from the straight line relationship except for the (220) reflection. In B.C.C. metal, faults should appear preferentially on {112} planes. Pure iron has a low stacking fault probability [Stacking Fault Energy [57,58] of iron $\simeq$ 140 ergs/cm^2]. Brandon and Nutting[59] suggest that the diffuse wavy slip bands observed in iron provide direct confirmation for both the ease of cross slip of the individual dislocations and the occurrence of slip in broad bands. So, the contribution to line shifts due to stacking faults can be ruled out.

The fact that with the exception of the weak (220) reflection, there is no significant departure from the straight line suggests that there is no contribution from the different yield properties of differently oriented grains. In other words, Heyn [intergranular] stresses are not significant.

4. SUMMARY AND CONCLUSIONS.

1. The lattice strain measured by X-rays as well as the total strain measured by strain indicator are proportional to the stress upto the limit of proportionality [about 12 x 10^3 psi].

2. Above the limit of proportionality, the lattice strain follows a cyclic variation with increase in plastic strain. A tentative hypothesis involving several processes contributory to such a phenomenon has been proposed.

3. The gradual unloading line for the lattice strain is found to be parallel to the loading line resulting in a RLS [e_z] which is compressive [in a direction perpendicular to that of pulling] and this is contrary to the hypothesis of Cullity[19].

4. The RLS [e_z] subsequent to instantaneous unloading is found to be tensile. On aging at room temperature, this reverses to a compressive RLS in about 12 to 20 hours. This is in agreement with the earlier observation of Swaroop and Tangri[22] on nickel.

5. The anelastic recovery [about 0.1 x 10^{-4} in/in] of the total strain subsequent to gradual unloading over a period of about 12 hours is much less than that [0.3 x 10^{-4} in/in] following instantaneous unloading. This is attributed to the fact that part of the anelastic recovery occurs during the process of gradual unloading.

6. A study of the lattice strain effects subsequent to instantaneous unloading suggests that the reversal in the sign of the RLS subsequent to instantaneous unloading could be due to the annihilation of vacancies as well as the rearrangement of dislocations during aging at room temperature.

7. The X-ray background intensity does not show any significant variation with deformation even after 20% strain. While the dislocation tangles, clusters and cells formed during deformation are expected to contribute to the background intensity, the observed phenomenon might be attributed to the fine ferritic grain size of the specimens [10.45×10^{-4} cm.].

8. Plots of shifts in the positions of Bragg maxima subsequent to deformation, $\Delta(2\theta)$ as a function of $\tan \theta$ are all linear with no significant departure from linearity [except for the case of the (220) reflection]. It is concluded that there are no contributions due to the Heyn [intergranular] stresses and the stacking faults.

5. SUGGESTIONS FOR FUTURE WORK.

1. A comparative study of the lattice strain effects accompanying uniaxial deformation of pure iron and low carbon steels with various carbon contents.

2. (a) A thorough investigation of the lattice strains in single and bi-crystals in order to determine the contribution of intergranular stresses to the origin of the residual lattice strain.

(b) A study of the concomitant changes of dislocation structures during the various stages of deformation and relate them to (a) above.

(c) Correlation of surface slip structure with the internal dislocation structure.

3. A study of the lattice strains in binary alloys which show a variation in elastic stiffness coefficients with variation in composition followed by electron microscopic investigation of substructure.

4. (a) An accurate determination of the rate of annihilation of point defects subsequent to instantaneous unloading of polycrystalline metal through an improved technique and thus suggest a mode of annihilation of the point defects.

(b) A study of the concomitant change in dislocation structure with room temperature aging aimed at gaining more insight into the mechanism of reversal in the RLS subsequent to instantaneous unloading.

5. A study of lattice strain effects accompanying deformation of single crystals and polycrystals at low temperature in order to draw further conclusions regarding the role of the point defects.

BIBLIOGRAPHY

1. F. Wever and B. Pfarr, Mitt. K-Wilh-Inst. Eisenfarsch, 1933. vol. 15, p. 137.

2. F. Bollenrath, V. Hauk and E. Osswald, z.ver.dtsch. Ing, 1939, vol. 83, p. 129.

3. S. L. Smith and W.A. Wood, Proc. Roy, Soc. (London), Ser. A, 1941, vol. 178, p. 93.

4. ibid, J. Inst. Met., 1941, vol. 64, p. 315.

5. G. B. Greenough, Prog. Metal Physics, 1952, vol. 3, p. 190.

6. R. Glocker and H. Hasenmaier, Z. ver. dtsch. Ing. 1940, vol. 84, p. 825, as quoted by G. B. Greenough, Prog. Metal Physics, 1952, vol. 3, p. 192.

7. S. L. Smith and W.A. Wood, Proc. Roy. Soc. (London), Ser. A, 1944, vol. 182, p. 404.

8. R. I. Garrod, Nature, 1950, vol. 165, p. 241.

9. L. G. Finch, Nature, 1950, vol. 166, p. 508.

10. C. J. Newton and H. C. Vacher, Trans. TMS - AIME, 1955, vol. 203, p. 1193.

11. M. J. Donachie Jr. and J. T. Norton, Trans. TMS - AIME, 1961, vol. 221, p. 962.

12. R. I. Garrod and G. A. Hawkes, Brit. J. Appl. Physics, 1963, vol. 14, p. 422.

13. E. Macherauch and P. Muller, Z. Metallk., 1958, vol. 49, p. 324.

14. C. Leiber and E. Macherauch, Z. Metallk., 1961, vol. 52, p. 196.

15. V. Hauk, Z. Metallk., 1955, vol. 46, p. 33.

16. Unpublished discussion (1943) between Bragg, Orowan, Smith and Wood, as quoted by G. B. Greenough, Prog. Metal. Physics, 1952, vol. 3, p. 193.

17. J. H. Auld and G. B. Greenough, Acta Met., 1954, vol. 2, p. 209.

18. C. J. Newton, J. Res. Natl. Bur. Std., 1963, vol. 67C, p. 101.

19. B. D. Cullity, Trans. TMS - AIME, 1963, vol. 227, p. 356.

20. A. S. Keh and S. Weissmann, Electron Microscopy and Strenth of Crystals, Interscience Publishers, 1963, p. 231.

21. R. I. Garrod and R. A. Coyle, Trans. TMS - AIME, 1963, vol. 230, p. 519.

22. B. Swaroop and K. Tangri, Trans. TMS - AIME, 1969, vol. 245, p. 61.

23. R. D. Carnahan and J. E. White, Trans. TMS - AIME, 1964, vol. 230, p. 249.

24. A. L. Christenson and E. S. Rowland, A. S. M. Trans., 1953, vol. 45, p. 638.

25. R. E. Ogilvie, "Stress Measurement with X-ray Spectrometer", M. S. Thesis, M.I.T., 1952.

26. D. P. Koistinen and R. E. Marburger, A. S. M. Trans., 1959, vol. 51, p. 537.

27. F. E. Werner, Discussion to Reference No. 3.

28. Measurement of Stress by X-ray, TR-182, Information Report, The Society of Automotive Engineers, New York.

29. B. D. Cullity, Elements of X-ray Diffraction, Addison-Wesley Publishing Co. Inc., Reading, Mass., 1956, p. 203.

30. C. S. Barrett and T. B. Marsalski, Structure of Metals, 3rd Edition, McGraw - Hill Book Co., New York, 1966, p. 132.

31. L. G. Orlov, Soviet Physics - Solid State, 1968, vol. 9, No. 8, p. 1828.

32. R. N. Singh and K. Tangri, Metallurgical Transactions (in Press).

33. D. G. Brandon and J. Nutting, J. I. S. I., 1969, vol. 196, p. 160.

34. G. Bäro, H. Gleiter and E. Hornbogen, Materials Science and Engineering, 1968-69, vol. 3, p. 92.

35. T. E. Mitchell and R. L. Smialek, "Work Hardening", Met. Soc. AIME Conference, Nov, 1966, Gordon and Breach Publishers, New York, 1968, p. 376.

36. C. J. Newton, J. Res. Natl. Bur. Std., 1963, vol. 67C, p. 101.

37. H. Kressel, D. W. Short and N. Brown, Acta Met., 1967, vol. 15, p. 525.

38. C. Schumacher, W. Schule and A. Seeger, Z. Naturforsch, 1962, vol. 17a, p. 228.

39. W. Schule, J. Phys. Soc. Japan, 1963, vol. 18, suppl. III, p. 292.

40. F. Seitz, Advances in Physics, 1952, vol. 1, p. 269.

41. N. F. Mott, Phil. Mag., 1952, [vii], vol. 43, p. 1151; 1953, [vii], vol. 44, p. 187, p. 742.

42. H. G. van Bueren and P. Jongenburger, Nature, 1955, vol. 175, p. 544.

43. J. Friedel, "Les Dislocations", 1956: Paris (Gauthier Villars).

44. H. G. van Bueren, Acta Met., 1955, vol. 3, p. 519.

45. A. C. Damask and G. J. Dienes, Point Defects in Metals, p. 171, Gordon and Breach Publishers, New York, 1963.

46. R. O. Simmons and R. W. Baluffi, Phys. Rev., 1962, vol. 125, p. 862.

47. F. Seitz, Advances in Physics, 1952, vol. 1, p. 43.

48. A. S. Keh and S. Weissmann, Electron Microscopy and Strength of Crystals, Interscience Publishers, 1963, p. 241.

49. D. Kuhlmann-Wilsdorf and H. G. F. Wilsdorf, ibid, p. 575.

50. J. O. Stiegler and C. K. H. DuBose, Acta Met., 1967, vol. 15, p. 953.

51. G. L. Ivanova and L. G. Orlov, Soviet Physics - Solid State, 1969, vol. 11, No. 6, p. 1262.

52. W. Carrington, K. F. Hale and D. McLean, Proc. Roy. Soc., 1960, vol. A 259, p. 203.

53. B. L. Averbach and B. E. Warren, J. Appl. Phys., 1949, vol. 20, p. 1066.

54. W. H. Hall and G. K. Williamson, Proc. Phys. Soc., London, 1950, vol. B64, p. 937.

55. M. S. Paterson, J. Appl. Phys., 1952, vol. 23, p. 805.

56. D. Mitchell and A. P. Smith, Phil. Mag., 1962, vol. 7, p. 737.

57. P. B. Hirsch and H. M. Otte, Acta Cryst., 1957, vol. 10, p. 447, as quoted by N. I. Noskova, V. A. Pavlov and S. A. Nemnonov, Physics of Metals and Metallography, 1965, vol. 20, p. 920.

58. E. A. Aqua and C. N. Wagner, Phil. Mag., 1964, vol. 9, p. 565, as quoted by N. I. Noskova, V. A. Pavlov and S. A. Nemnonov, Physics of Metals and Metallography, vol. 20, p. 920.

59. D. G. Brandon and J. Nutting, Acta Met., 1959, vol. 7, p. 101.